# Micromap (μMap) Photoproximity Labeling for Integrated Phenotypic Screening and Accelerated Prioritization of Targeted Protein Degrader Compounds

**Steve D. Knutson**[1,2†], **Danielle C. Morgan**[1,2†], Ryan E. McNamee[1,2], Jack L. Sloane[3], Jonathan B. Olsen[4], Steven Levine[4], Gabe Mintier[4], Monica Kwok[4], Payal R. Sheth[4] & David W. C. MacMillan[1,2*]

[†]equal contributions
*corresponding author

[1]Department of Chemistry, Princeton University, Princeton, New Jersey, 08544, United States
[2]Merck Center for Catalysis at Princeton University, Princeton, New Jersey, 08544, United States
[3]Global Discovery Chemistry, Bristol Myers Squibb, Cambridge, Massachusetts, 02142, United States
[4]Discovery Biotherapeutics & Lead Discovery and Optimization, Bristol Myers Squibb, Princeton, New Jersey 08543, United States

**Phenotypic screening is a powerful tool for discovering first-in-class medicines, but its potential is limited by the significant challenge of triaging hit compounds and deconvoluting their mechanisms. [1,2] Similarly, targeted protein degradation (TPD) represents a powerful new therapeutic strategy but is constrained by its reliance on a small number of E3 ligases with limited capability to discover new degradation mechanisms within validated platforms.[3] Here, we present an integrated platform that bridges phenotype and mechanism, enabling rapid prioritization and characterization of small molecule hits from high throughput screening with sequential proximity labeling technologies. First, immunophotoproximity labeling (μMapX) is used to profile drug-induced interactome changes of an endogenous protein target to rapidly triage hits displaying discrete or promising mechanisms. Second, photocatalytic μMap target identification (μMap TargetID) is used to characterize protein engagement for candidate compounds and provide orthogonal mechanistic insight. As a test case, we applied this platform to discover degraders of BTB and CNC Homolog 2 (BACH2), a key immunoregulatory transcription factor.[4] This approach rapidly prioritized a lead compound scaffold that inhibits GSK3β to induce proximity between β-catenin and BACH2, leading to its degradation through a LON peptidase-dependent mechanism. Together, this integrated platform provides a generalizable strategy to accelerate drug discovery by de-risking and prioritizing phenotypic hits, discovering degraders with novel mechanisms, and uncovering therapeutically targetable biology.**

Small molecule drug discovery is a cornerstone of modern biomedicine. However, the path to a clinically approved therapeutic is marked by high attrition rates and significant investment, with the average cost per asset exceeding $2.2 billion.[5] To circumvent these challenges, the past decade has seen a significant resurgence in phenotypic drug discovery (PDD).[2,6] Unlike target-based approaches constrained by a predefined hypothesis, this "biology-first" strategy can uniquely reveal compounds that act via previously unknown targets or novel mechanisms-of-action (MoA) to expand the therapeutic landscape. These advantages underlie the prevalence of recent PDD campaigns, which have yielded many recent first-in-class medicines, including CFTR potentiators,[7] pre-mRNA splicing modifiers for spinal atrophy,[8] anti-viral NS5A inhibitors,[9] and Bromodomain modulators in cardiovascular disease.[10]

In parallel, the field of targeted protein degradation (TPD) has emerged as a revolutionary therapeutic modality to target previously "undruggable" proteins.[3] However, TPD also faces major limitations; the discovery of degraders that utilize new mechanisms is often a matter of serendipity, and these drugs are primarily reliant on the E3 ubiquitin ligases cereblon (CRBN) and Von Hippel-Lindau (VHL). Applying PDD to discover new degraders or degradation mechanisms remains a significant challenge, as even a single high-throughput campaign yields dozens to hundreds of candidates with no rational means to triage or prioritize which hits warrant further investigation.[11,12] This "target deconvolution" bottleneck to identify the molecular basis for compound activity remains one of the most resource-intensive and frequently unsuccessful processes in drug development.[13] Moreover, while PDD hits can be empirically optimized to yield development candidates, incomplete understanding of a compound's MoA at the developmental stage often leads to failures in later clinical trials.[6,14]

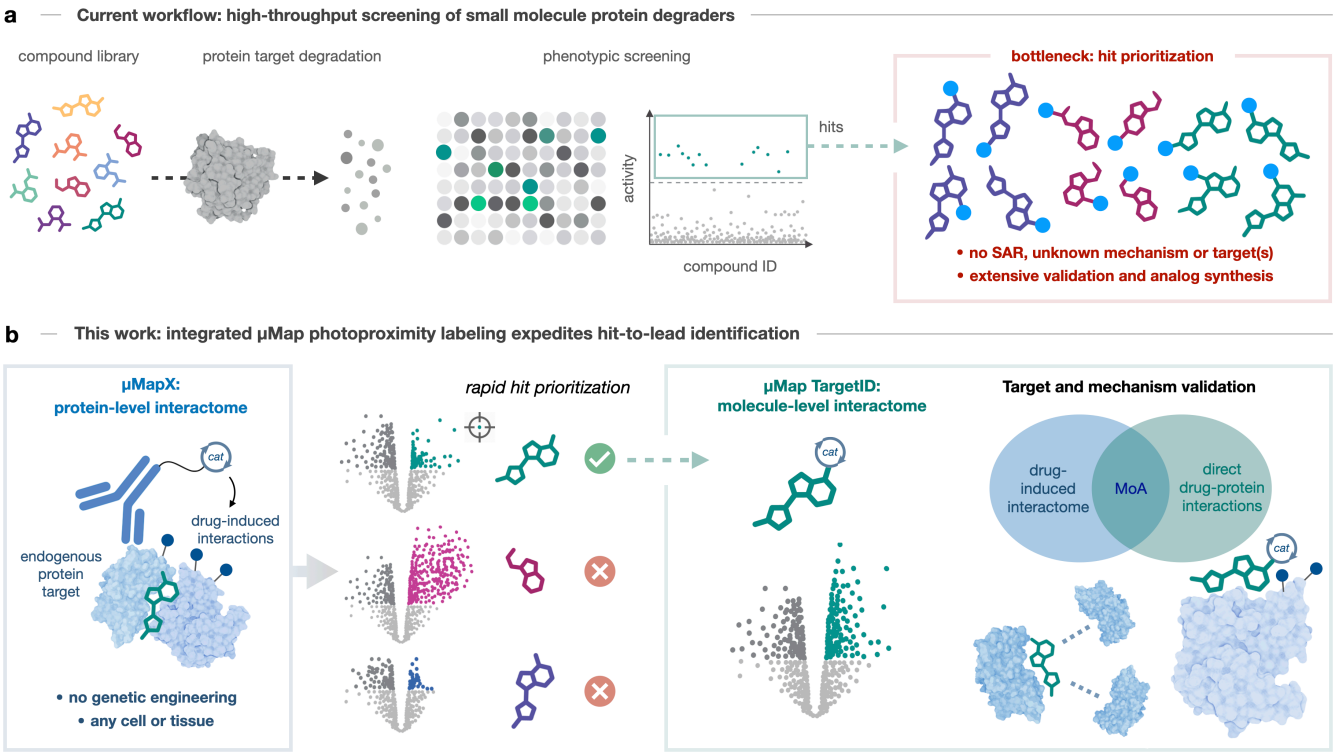


**Figure 1 | Integrated µMap photocatalytic proximity labeling streamlines protein degrader discovery.** (a) Phenotypic screening for degraders identifies numerous "hits" that induce the desired phenotype but provide no MoA or SAR information. This creates a "hit prioritization bottleneck," requiring resource-intensive validation and analog synthesis to select viable leads. (b) Sequential µMap workflow with µMapX immunophotoproximity labeling profiles the drug-induced changes to the target protein's immediate interactome, enabling rapid prioritization of compounds with on-pathway signatures. µMap TargetID is then employed on candidate compounds, providing secondary target engagement data and elucidation of additional molecular machinery to accelerate MoA identification.

Proximity labeling has emerged as a powerful strategy to uncover complex biological mechanisms by mapping biomolecular interactions in their native cellular context. This approach is particularly well-suited to address challenges in both degrader discovery and phenotypic screening, where deconvolution of a compound's target and MoA can be elucidated through chemoproteomic interaction analysis. Our laboratory has recently developed a high-resolution proximity labeling platform termed microenvironment mapping (µMap),[15] wherein photocatalysts are activated with light to generate carbene species from diazirine-based probes.

These highly reactive carbenes ($T_{1/2}$ ~1 ns) covalently modify proximal biomolecules within a small radius (~2 nm), affording unparalleled spatiotemporal resolution for mapping interaction networks.[16] We have deployed µMap in a variety of biological settings, including immune synapses and cell-surface receptor networks,[15,17-19] oncogenic chromatin remodeling events,[20] and phase-separated condensates in living cells.[21,22] Critically, high-resolution µMap can also identify small-molecule drug targets and map their binding sites with amino-acid-level resolution.[23,24] We also recently demonstrated immunophotoproximity labeling in formalin-fixed paraffin-embedded slides (µMap-FFPE),[25] unlocking high-resolution interactomic capabilities toward endogenous protein targets in primary patient tissues.

Here, we adapt and integrate two µMap platforms to systematically bridge the gap between drug phenotype and mechanism. Our strategy combines high-throughput PDD with sequential, high-resolution proximity labeling technologies to deconvolute hit MoAs, enabling rapid triage and prioritization of candidate compounds based on their induced interactomes. We then utilize photocatalytic µMapTarget ID to assess direct target engagement and elucidate the molecular machinery involved in each MoA. As a vanguard application of this platform, we investigate degraders of BACH2, a master immunoregulatory transcription factor. Our approach rapidly prioritized a lead compound scaffold that inhibits GSK3β and induces proximity between BACH2 and β-catenin, culminating in apparent degradation through the protease LONP1. This demonstration highlights the integrated µMap platform as a novel method to accelerate drug discovery by de-risking phenotypic hits while uncovering new, therapeutically actionable biology in protein degrader development.

## Platform Conceptualization

Conventional PDD campaigns begin with an activity-based screen to identify compounds that produce a desired biological outcome, such as the degradation of a specific protein target (**Fig. 1a**). While effective at generating initial hits, this process invariably leads to a "prioritization bottleneck," wherein dozens or hundreds of compounds exhibit desired activity yet contain no information about molecular target(s) or MoA. Hit deconvolution with photoaffinity labeling and chemoproteomics requires bespoke synthesis of functionalized analogs for each compound series.[26-28] This process is particularly arduous for phenotypic hits, which upon discovery lack any structure-activity relationship (SAR) data to guide probe design, often resulting in the synthesis of hundreds of compounds to find a single viable tool for TargetID. Even after navigating this synthetic challenge and verifying functional bioactivity of each analog, subsequent investigation of even a few hit compounds requires significant additional resources to biochemically probe relevant cellular pathways and validate potential MoAs.

We envisioned that an integrated µMap platform could directly address this challenge by systematically bridging the gap between phenotype and mechanism (**Fig. 1b**), enabling rational de-risking and selection of the most promising candidates for eventual optimization. The workflow begins with µMap in cross-linked cells (µMapX), utilizing antibody-directed immunophotoproximity labeling to rapidly fingerprint drug-induced interactomes for each hit compound. By profiling these changes in the endogenous protein target's microenvironment, we can swiftly triage initial hits to prioritize those that exhibit qualitatively clean, on-pathway, or promising signatures while deprioritizing compounds with convoluted or non-selective mechanisms. We can then employ µMap TargetID to provide secondary validation of MoA by profiling direct molecule–protein engagement involved in the drug mechanism. This integrated, two-step approach translates hit prioritization from serendipitous exploration into a rapid, unbiased, data-driven strategy, significantly accelerating the discovery of novel therapeutics.

## High-throughput Phenotypic Screening for BACH2 Degrader Compounds

As a demonstration of our platform, we pursued the discovery of novel degraders for BACH2, a master transcriptional repressor with high therapeutic value in immunology and oncology.[4] BACH2 is a key regulator of lymphocyte differentiation and quiescence, and its degradation is a critical step for immune activation, making it an attractive target for therapeutic intervention.[29-31] To screen compounds, we engineered a human kidney cell line (HK-2) to endogenously tag BACH2 with an 11-amino-acid HiBiT peptide. This system provides a highly sensitive luminescent readout directly proportional to endogenous BACH2 protein levels, making it ideal for high-throughput evaluation.[32] We screened a large small-molecule library, identifying a focused group of 10 compounds with sufficient material, chemical stability, and overall purity for confirmation assays and further mechanistic investigation (**Fig. 2**). These hits were subjected to a counter screening cascade to filter out compounds displaying non-selective mechanisms or broad toxicity. Several compounds were initially flagged based on this analysis, including 9 which displayed high HiBiT degradation potency but was virtually unaffected by proteasomal inhibition with MG132. **1**, **6** and **3** were similarly deprioritized. **2** and **7** displayed weak degradation potencies ($DC_{50}$ > 7 µM), while **10** was observed to have both low activity and a narrow therapeutic window, with significant cytotoxicity observed at concentrations close to $DC_{50}$ values. In contrast, **8** and structurally similar chemotypes **4/5** demonstrated potent, sub-µM degradation of endogenous BACH2, clear proteasome dependence (+MG132 $DC_{50}$ > 30 µM), and a wide therapeutic window with minimal impact on cell viability ($IC_{50}$ > 30 µM).

To further evaluate compound hits, we also assessed degradation of endogenous, untagged BACH2 in a therapeutically relevant Jurkat T cell lymphoma line via Western blotting. In alignment with HiBiT assay data, we prioritized the three most potent and mechanistically clean compounds **8** and sister compounds **4/5**, which demonstrated robust, dose-dependent degradation of endogenous BACH2. Conversely, a number of compounds were de-prioritized, including **2**, **3**, **7**, and **9**, which showed no significant reduction in endogenous BACH2 levels, even at high concentrations. Interestingly, compounds **1** and **6** and clearly induced the loss of BACH2 protein, yet our previous characterization showed that activity was not repressed by proteasome inhibition. We recognized that these hits presented a unique opportunity to utilize our integrated µMap platform to confirm or refute potential non-canonical degradation pathways. Therefore, we selected these compounds alongside proteasome-dependent hits for sequential µMap analysis to rapidly assess their drug-induced interactions and potential MoAs.

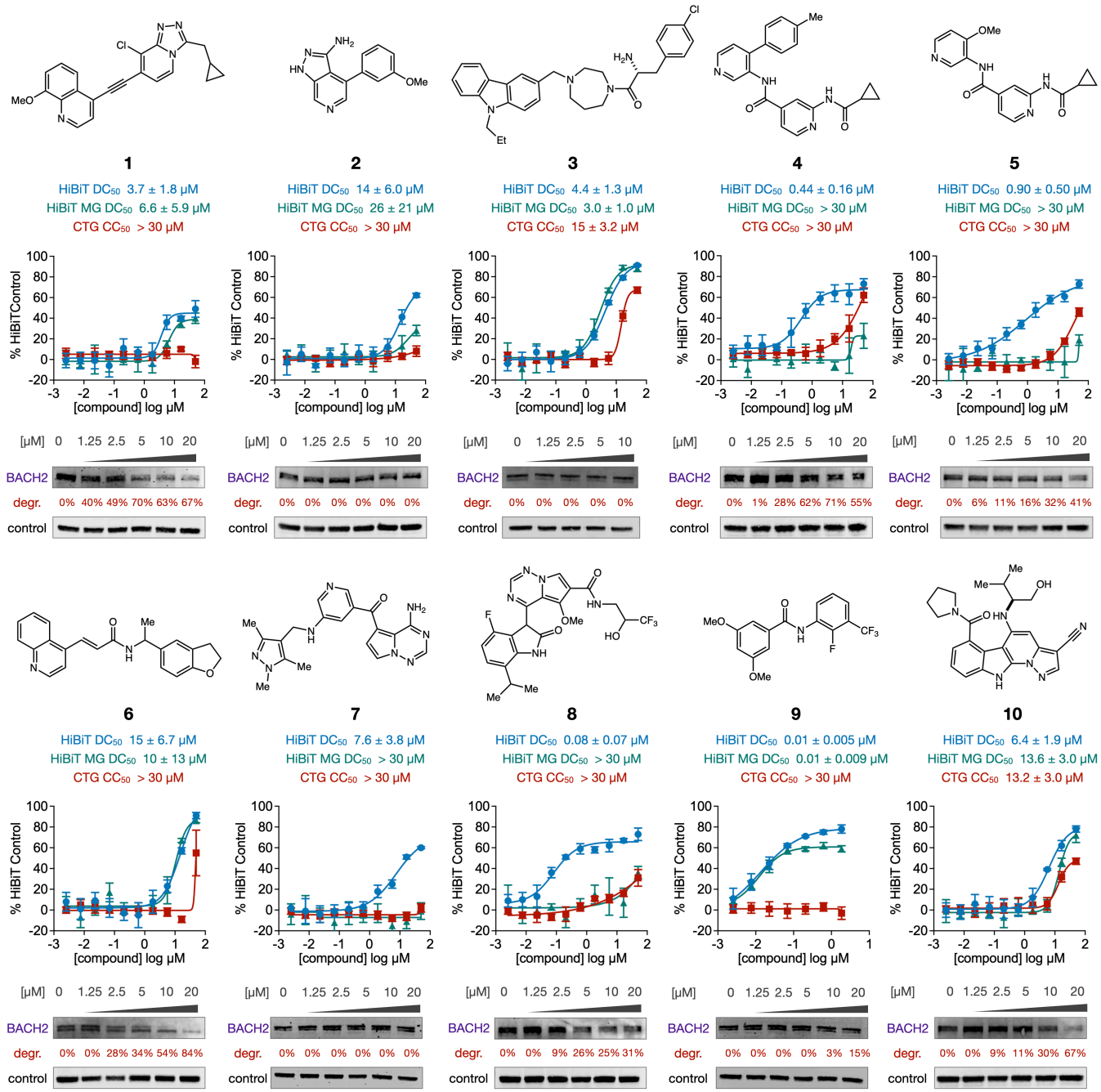


**Figure 2 | Representative BACH2 degrader chemotypes selected from a high-throughput phenotypic screen.** 10 compounds were selected for initial biochemical evaluation. Dose-response curves depict BACH2 degradation as measured by HiBiT assay (blue), in the presence of MG132 (green), and cytotoxicity as measured by the CellTiter-Glo (CTG) assay (red). Mean $DC_{50}$ (degradation) and $CC_{50}$ (cytotoxicity) values are derived from curve fitting with 95% confidence intervals. Western blot analyses were performed to validate endogenous BACH2 degradation in Jurkat T cells following overnight treatment with increasing concentrations (0–20 μM) of each compound. Densitometric quantification of percent degradation relative to the vehicle control is shown below each blot.

## μMapX Profiling of Drug-Induced BACH2 Interactomes

To rank the five prioritized compounds and gain deeper mechanistic insight, we established an immunophotoproximity workflow to map the endogenous BACH2 interactome directly in chemically crosslinked Jurkat T cells (μMapX). We drew inspiration from our recently developed μMap-FFPE platform,[25] which enables high-resolution interactome mapping of endogenous protein targets in formalin-fixed tissue slides. In this application, a BACH2-specific primary antibody is used to recruit a secondary antibody conjugated with a Sn-chlorin photocatalyst to facilitate light-induced biotinylation of BACH2 and any drug-induced interactors for subsequent enrichment and quantitative mass spectrometry.[33] We first performed a baseline μMapX experiment in

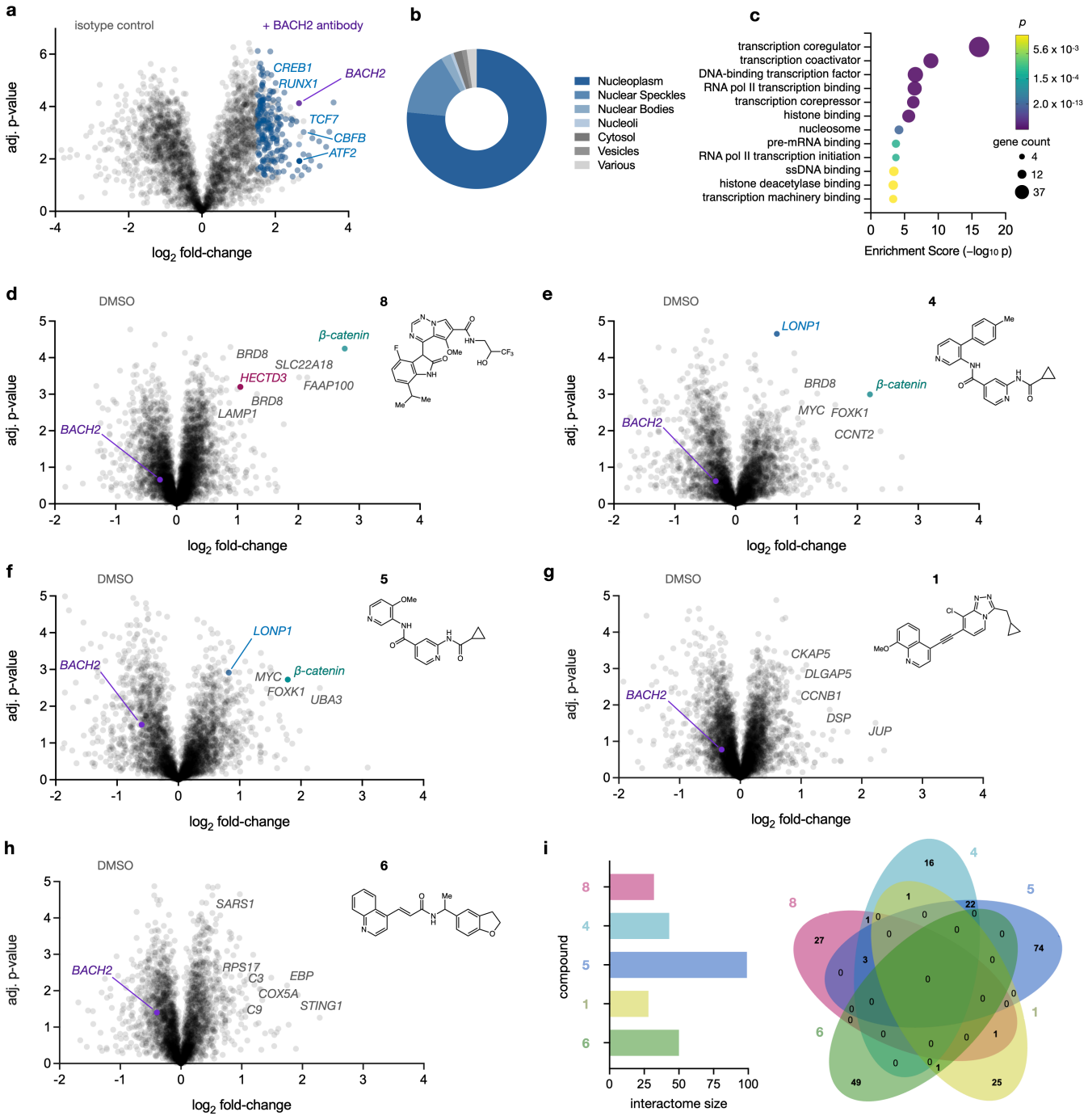


**Figure 3 | Profiling drug-induced BACH2 interactome changes with µMapX.** (a) Volcano plot of quantitative µMapX proteomics of endogenous BACH2 in untreated Jurkat cells. Selected known interactors are labeled, with nuclear annotated proteins (blue). (b) Donut plot of subcellular localization of identified BACH2-proximal proteins ($log_2FC > 1.5$, $p < 0.05$). (c) GO enrichment analysis of BACH2 interactors. (d-h) Volcano plots of drug-induced BACH2 interactomes. (i) Comparative analysis of drug-induced interactomes. Bar chart (left) illustrates total number of significantly enriched ($log_2FC > 0.75$) proteins for each compound. Venn diagram (right) illustrates the distinct profiles of the ambiguous compounds and convergent overlap of the prioritized degraders.

untreated, crosslinked Jurkat cells to validate our method. Quantitative proteomic analysis demonstrated high specificity and accuracy, with BACH2 itself significantly enriched along with several known transcriptional interactors RUNX1, ATF2, TCF7, CBFB and CREB1 (**Fig. 3a**).[34-36] Subcellular annotation of interactors demonstrated ~95% of identified proteins localized to nuclear compartments (**Fig 3b**).[37] Functionally, gene

ontology (GO) analysis of proximal proteins revealed strong enrichment for transcriptional regulation, chromatin binding, and RNA processing (**Fig. 3c**), consistent with its established roles in regulating gene expression.[29,31]

With these data providing a robust baseline map of the endogenous BACH2 interactome, we next applied μMapX to profile drug-induced interactions of the five selected hits: three proteasome-dependent degraders (**4, 5, 8**) and two mechanistically ambiguous hits (**1, 6**). Recapitulating $DC_{50}$ values from our western blotting analysis (**Fig. 2**), Jurkat cells were treated with ~10-20 μM of each compound overnight and then immediately crosslinked to preserve drug-induced interactions. μMapX proteomics of **4**, **5**, and **8** revealed a convergent mechanistic trend, with β-catenin robustly enriched upon drug treatment (**Figs. 3d-f).** In contrast, **1** induced a disparate interactome (**Fig. 3g**), including cell cycle regulation (CKAP2, DLGAP5, CCNB1) and cell-cell adhesion proteins (DSP, JUP), potentially indicative of stress response and non-specific protein loss rather than targeted degradation. Similarly, 6 enriched proteins involved in immune response (STING1), the complement cascade (C3, C9), and protein synthesis (SARS1, RPS17), suggesting a broad homeostatic or non-specific inflammatory response (**Fig. 3h**). We were thus able to quickly deprioritize both compounds due to their complex interactions and likelihood for pharmacologically intractable mechanisms.

Interactome meta-analysis revealed distinct patterns of protein enrichment for each compound (**Fig 3i**). Consistent with their mechanistic ambiguity, **1** and **6** displayed minimal overlap between themselves or with the other compounds. **4** and **5**, which share a nearly identical scaffold, induced similar interactomes, sharing 22 proximal proteins exclusively. This high overlap between structurally related compounds provided additional validation that the observed interactome changes are a direct and specific consequence of the chemical matter. Together, the three proteasome-dependent degraders (**4**, **5**, and **8**) commonly enriched β-catenin, BRD8, and FOXK1. The shared enrichment of β-catenin, a key component of the Wnt signaling pathway,[38] and FOXK1, a known regulator of Wnt/β-catenin signaling,[39] suggested a convergent MoA involving the modulation of this cell-fate pathway. No canonical E3 ligases were enriched aside from HECTD3 upon treatment with **8** (**Fig. 3d**), and when we tested BACH2 degradation in HECTD3 knockout (KO) Jurkat cells, we did not observe rescue of degradation (**Fig. S1**). However, compounds **4/5** both induced significant enrichment of LONP1 (**Fig. 3e,f**), potentially mediating BACH2 stability through a non-canonical pathway involving the ATP-dependent protease. Overall, this panel of experiments enabled us to rapidly deprioritize ambiguous hits and prioritize **4**, **5** and **8** chemotypes for their specific and mechanistically intriguing profiles.

## Identifying Protein Targets of Small Molecule BACH2 Degraders

μMapX provides a BACH2-centric rationale for compound prioritization but does not identify the direct molecular binding partner(s) of the small molecules themselves. We thus advanced the three lead compounds to μMap TargetID analysis,[23] where Ir photocatalysts are directly conjugated to small molecule hit analogs to enable photocatalytic biotinylation of direct drug binding partners within living cells. The catalytic nature of μMap TargetID allows for significant signal amplification, overcoming the limitations of traditional stoichiometric techniques like photoaffinity labeling (PAL). We first synthesized Ir-conjugated versions of the lead compounds, starting from **8** using the trifluoro-hydroxypropyl amide moiety as a synthetically tractable vector for photocatalyst conjugation (**Fig. 4a**). Based on the shared chemotype between **4** and **5**, which only differ by a p-tolyl versus methoxy-pyridinyl moiety, a single representative conjugate was synthesized leveraging this conjugation vector (**Fig. 4b**). After verifying functional ability of these analogs to degrade BACH2, we then profiled their direct protein-level interactomes.

μMap TargetID of **8** yielded a small and heterogeneous interactome, including RNA-binding proteins IGF2BP2 and PCBP2, transcriptional coactivator MED14, cytoskeletal component PLS1, and solute carrier (SLC) SLC16A7 (**Fig. 4a**). To rule out transcriptional silencing as a potential mechanism of **8**, we measured BACH2 mRNA levels after treatment with each compound and did not observe significant decreases in transcript abundance (**Fig. S2**). The presence of an SLC transporter could suggest a mechanism for cellular uptake, but the overall profile lacked a clear mechanistic thread that could explain the convergent enrichment of β-catenin seen in μMapX experiments. Most importantly, the absence of BACH2 in our dataset likely rules out the possibility that **8** functions as a direct binder or molecular glue.

In parallel, we performed μMap TargetID for the **4/5** chemotype (**Fig. 4b**). While we also observed SLCs potentially involved in drug transport, we observed striking enrichment of GSK3β (Glycogen Synthase Kinase 3 Beta), the central kinase that phosphorylates β-catenin to mark it for proteasomal degradation and maintain low protein levels in the absence of Wnt signaling.[38] Upon inhibition of phosphorylation through Wnt activation, β-catenin can diffuse into the nucleus and activate gene expression. BACH2 was once again absent from our dataset, suggesting these compounds also do not engage as direct binders or glues. Rather, these data implicate

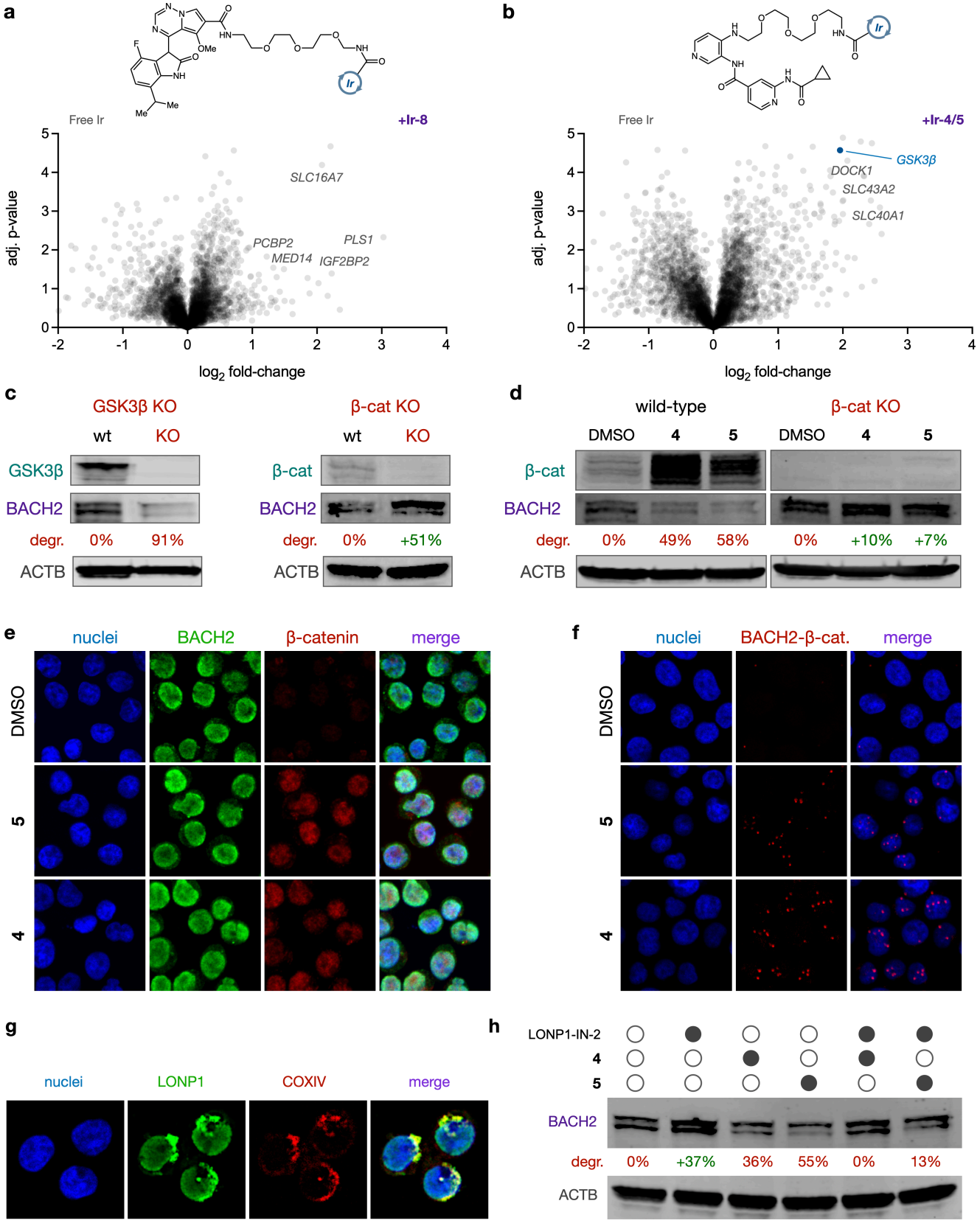


**Figure 4 | µMap TargetID reveals compounds 4 and 5 inhibit GSK3β.** (a,b) Chemical structures of Ir conjugates for 8 and 5 and volcano plots of µMap TargetID enrichment of protein interactors. (c) Western blot analysis of BACH2 following CRISPR KO of Wnt pathway components. (d) Drug-induced BACH2 degradation in wild-type and β-catenin KO cells. (e) Immunofluorescence microscopy of drug-induced nuclear accumulation of β-catenin (red) and co-localization with BACH2 (green) in the nucleus (DAPI, blue). (f) Proximity ligation assay for detecting BACH2 and β-catenin interactions. (g) Immunofluorescence microscopy of LONP1 (green) co-localization with mitochondria (red) and the nucleus (DAPI, blue). (h) Drug-induced degradation of BACH2 under LONP1 inhibition.

their action as GSK3β inhibitors to prevent β-catenin phosphorylation and promote its nuclear accumulation, supporting the observed drug-induced proximity with BACH2 in our initial μMapX experiments. This testable hypothesis immediately prioritized the **4/5** series for further biochemical validation, while the more convoluted profile of **8** suggested a higher-risk, polypharmacological mechanism.

## Compounds 4 and 5 Inhibit GSK3β

To initially explore the relationship between BACH2 stability and Wnt signaling, we generated KOs of both GSK3β and β-catenin in Jurkat cells. Genetic ablation of GSK3β led to a profound decrease (91%) in BACH2 protein levels (**Fig. 4c**), recapitulating hit compound effects implicating GSK3β inhibition as an upstream trigger for BACH2 downregulation. Reciprocal KO of β-catenin displayed upregulated BACH2 levels (+52%), supporting the hypothesis that β-catenin is a downstream mediator of BACH2 stability. We next pharmacologically validated this mechanism by treating wild-type cells with either **4** or **5**, and we observed a dramatic increase in the steady-state levels of β-catenin that correlated with the concomitant degradation of BACH2 (**Fig. 4d**). We also compared our lead compounds with two commercially available GSK3β inhibitors, TWS-119 and HY-130795 (**Fig. S3**).[40,41] Both **4** and **5** induced degradation of BACH2 that correlated with increased levels of both total and active (non-phosphorylated) β-catenin. Importantly, this phenotype was reproduced by TWS-119, a structurally orthogonal GSK3β inhibitor that induced robust BACH2 degradation (71%). This further supports that degradation of BACH2 is a downstream consequence of GSK3β inhibition.

HY-130795 is a structurally similar analog to our lead chemotypes, featuring a thiazole-carboximide core in place of the 4-substituted pyridine scaffold. This analog initially appeared inactive at a 20 μM dose, but this was also accompanied by notable cytotoxicity. Upon titration of HY-130795, we observed a dose-dependent increase in active β-catenin that correlated with BACH2 downregulation at nanomolar concentrations (**Fig. S4**). Collectively, the fact that our lead chemotypes, in addition to analogous HY-130795 and structurally orthogonal TWS-119, all promote both β-catenin stabilization and BACH2 degradation provides pharmacological evidence for our proposed MoA. HY-130795 induces BACH2 degradation at nanomolar concentrations, indicating that the thiazole-based scaffold is more potent and provides an efficient starting point to optimizing for GSK3β inhibition.

We next tested whether β-catenin was required for compound activity by comparing their effects in β-catenin KO Jurkat cells (**Fig. 4d**). Compared with wild-type cells, the compounds had minimal effect on BACH2 levels, providing genetic evidence that β-catenin is an essential component of the drug-induced degradation pathway. We next visualized drug-induced changes to β-catenin localization using immunofluorescence microscopy (**Fig. 4e**). As expected, β-catenin levels are low in the basal state (vehicle), while BACH2 was consistently observed in the nucleus. Upon treatment with either **4** or **5**, accumulation and nuclear translocation of β-catenin was observed with co-localization with BACH2. To validate drug-induced proximity between BACH2 and β-catenin *in situ*, we performed a proximity ligation assay (PLA) (**Fig. 4f**), which generates a fluorescent signal only when two target proteins are within very close proximity (~40 nm).[42] While control treatment (vehicle) showed only background signal, cells treated with either **4** or **5** displayed a dramatic increase in distinct nuclear puncta, indicating a close physical association between BACH2 and β-catenin. Together, these experiments demonstrate that our lead compounds function by inhibiting GSK3β, in turn stabilizing β-catenin, leading to its nuclear accumulation, and promoting interaction with BACH2 for its subsequent degradation.

## LONP1 is Required for Drug-induced BACH2 degradation

Lastly, we investigated the functional role of LONP1, an ATP-dependent serine protease identified as a drug-induced interactor for the **4/5** chemotype in our μMapX screen. This finding was initially surprising, as LONP1 has been long characterized as a mitochondrial peptidase,[43] although recent work has identified nuclear residence in human and murine cells under normal conditions.[44,45] Additionally, recent precedent has shown that nuclear LONP1 directly regulates the levels of the transcription factor Heat Shock Factor 1 (HSF1), particularly in response to cellular stress.[45] We first confirmed subcellular localization of LONP1 in wild-type Jurkat cells, and immunofluorescence microscopy revealed co-localization with both the mitochondrial marker COXIV as well as the nucleus (**Fig. 4g**). To test whether LONP1 is functionally required for BACH2 degradation, we utilized a LONP1-specific inhibitor, LONP1-IN-2 (**Fig. 4h**).[46,47] Treatment with the inhibitor alone (1 μM) resulted in a 37% increase in basal BACH2 levels, suggesting that LONP1 is involved in the constitutive stability of BACH2 and that our compounds may enhance a pre-existing degradation pathway rather than creating one *de novo*. Treatment with either **4** or **5** alone expectedly resulted in degradation of BACH2, but co-treatment with the LONP1 inhibitor abrogated or significantly reduced this degradation. Together, these data provide strong pharmacological evidence that the proteolytic activity of LONP1 is essential for the downstream degradation of BACH2. The initial

observation that MG132, a proteasome inhibitor, rescued BACH2 from degradation was a key criterion that led us to prioritize these compounds, as it suggested a canonical, proteasome-dependent degradation mechanism. Global proteasome inhibition can induce a complex, indirect effect on the Wnt pathway, but it is also known that MG132 and bortezomib directly inhibit LONP1,[47,48] providing a direct rationale for our initial observed results. β-catenin has also been recently implicated in regulating the stability of intrinsically disordered transcriptional proteins,[49] and we hypothesize that the induced interaction with BACH2 may trigger a significant conformational change. This structural rearrangement could expose a previously shielded degron on BACH2, thereby marking it for recognition and degradation by LONP1, which is known to target conformationally altered or unfolded proteins.[50-52] The precise molecular communication between the nuclear BACH2/β-catenin complex and LONP1 is an intriguing area for future investigation, and its discovery highlights the power of our platform to uncover new, therapeutically relevant biology.

## Discussion

The development of new medicines is challenged with high attrition rates, and this is often driven by incomplete understanding of how a small molecule functions within the complex cellular ecosystem. PDD offers a powerful strategy to navigate this complexity by identifying compounds based on a desired biological outcome, yet it is significantly limited by the "target deconvolution bottleneck" where identifying a hit's MoA is arduous and often unsuccessful. Concurrently, the field of TPD has revolutionized therapeutic possibilities but remains largely dependent on a small fraction of the cell's degradation machinery, making the discovery of novel modalities a matter of serendipity. In this work, we present an integrated µMap technology platform that confronts these parallel challenges, shaping a direct, rapid, and data-driven path from cellular phenotype to actionable molecular mechanism.

Conventional PDD deconvolution often requires the bespoke synthesis of numerous functionalized analogs for each of the dozens to hundreds of hits from a phenotypic screen, a resource-intensive process needed for traditional target ID methods like photoaffinity labeling. Even after this synthetic effort, the selection of a few candidates for the arduous biochemical validation required to prove a mechanism remains a significant hurdle. Our approach inverts and streamlines this paradigm by first employing µMapX immunophotoproximity labeling as a primary triage tool to generate an interactomic fingerprint for every hit parental compound at the outset. This allows for rapid prioritization of compounds with "clean," on-pathway signatures, as demonstrated by our ability to distinguish the discrete interactomes of **4**, **5**, and **8** from the complex, pleiotropic profiles of **1** and **6**. This ability to triage problematic compounds early in the process fundamentally de-risks a drug discovery program and increases the potential of PDD to deliver first-in-class medicines.

Secondary screening using µMap TargetID to profile small molecule-protein interactions further highlighted the utility of this integrated platform through orthogonal deconvolution of our lead chemotype's MoA. The initial null hypothesis—that we had discovered direct BACH2 degraders—was quickly refuted by µMap Target ID, where BACH2 was absent among direct binding partners. This critical negative result, which would have been difficult and time-consuming to obtain with traditional methods, prevented us from pursuing this flawed hypothesis. Instead, this process rapidly pinpointed GSK3β as the direct target of the **4**/**5** series. This provided a testable, unifying hypothesis supported by subsequent experiments showing that direct inhibition of GSK3β leads to the stabilization and nuclear accumulation of β-catenin, in turn promoting proximity to BACH2 and its subsequent degradation. This cascade confirmed a previously unknown regulatory axis connecting the canonical Wnt pathway to the stability of a master immune regulator BACH2. While it is conceivable that we would have determined that our series targeted GSK3β via conventional kinome inhibition panels,[53] building the connectivity of this molecular target with its action on β-catenin would have been far beyond the capacity of these assays.

The unexpected but consistent enrichment of LONP1 in our µMapX screens also revealed a non-canonical degradation pathway involving the mitochondrial protease LONP1. Our results support recent studies showing nuclear localization of LONP1 to regulate the stability of nuclear transcription factors.[44,45] Our finding reveal that LONP1 activity is essential for BACH2 degradation, and that its inhibition leads to an increase in basal BACH2 levels, suggests our compounds exploit or enhance a pre-existing LONP1-dependent pathway for BACH2 turnover. This finding expands the known toolkit for TPD beyond the ubiquitin-proteasome system and opens up new areas of biological inquiry into how additional proteases can regulate the fate of nuclear proteins.

Together, the integrated µMap platform described in this work provides a robust and generalizable engine for modern drug discovery. It directly addresses the critical PDD bottleneck of target deconvolution, while simultaneously providing a rational path to discover and characterize therapeutics with new mechanisms of action. This demonstration workflow to discover BACH2 degraders highlights the integrated µMap platform as a powerful

method to accelerate drug discovery by de-risking phenotypic hits uncovering new, therapeutically actionable biology. By transforming the risk of a phenotypic screen into an opportunity for mechanistic and biological discovery, this integrated μMap approach can facilitate the next generation of innovative medicines.

## AUTHOR INFORMATION


Corresponding Author

**David W. C. MacMillan** – Department of Chemistry, Princeton University, Princeton, New Jersey, 08544, USA; Merck Center for Catalysis at Princeton University, Princeton, New Jersey 08544, United States; orcid.org/0000-0001-6447-0587;
Email: dmacmill@princeton.edu

**Authors**

**Steve D. Knutson** – Department of Chemistry, Princeton University, Princeton, New Jersey, 08544, USA; Merck Center for Catalysis at Princeton University, Princeton, New Jersey 08544, USA

**Danielle C. Morgan** – Department of Chemistry, Princeton University, Princeton, New Jersey, 08544, USA; Merck Center for Catalysis at Princeton University, Princeton, New Jersey 08544, USA

**Ryan E. McNamee** – Department of Chemistry, Princeton University, Princeton, New Jersey, 08544, USA; Merck Center for Catalysis at Princeton University, Princeton, New Jersey 08544, USA

**Jack L. Sloane** – Global Discovery Chemistry, Bristol Myers Squibb, Cambridge, Massachusetts, 02142, United States

**Jonathan B. Olsen** – Discovery Biotherapeutics & Lead Discovery and Optimization, Bristol Myers Squibb, Princeton, New Jersey 08543, United States

**Steven Levine** – Discovery Biotherapeutics & Lead Discovery and Optimization, Bristol Myers Squibb, Princeton, New Jersey 08543, United States

**Monica Kwok** – Discovery Biotherapeutics & Lead Discovery and Optimization, Bristol Myers Squibb, Princeton, New Jersey 08543, United States

**Payal Sheth** – Discovery Biotherapeutics & Lead Discovery and Optimization, Bristol Myers Squibb, Princeton, New Jersey 08543, United States


**Data availability**

All data supporting the findings of this study are available in the main text or in the Supplementary Information.

**Competing interests:** D. W. C. M. declares an ownership interest in the Penn PhD photoreactor, which is used to irradiate samples in this work. D.W.C.M declares an ownership interest in the company Dexterity Pharma LLC, which has commercialized materials used in this work. The other authors declare no competing interests.


**Acknowledgements:** Research reported in this work was supported by the Princeton Catalysis Initiative and Bristol Myers Squibb. S.D.K. acknowledges the NIH for postdoctoral fellowships (1F32GM142206 and 1K99GM154140). We would also like to thank Gary S. Laevsky and Sha Wang of the Confocal Imaging Facility, a Nikon Center of Excellence, in the Department of Molecular Biology at Princeton University for instrument use and technical advice. Illustrations were created with BioRender.com.

## REFERENCES


1 Brown, D. G. An analysis of successful hit-to-clinical candidate pairs. *Journal of medicinal chemistry* **66**, 7101-7139 (2023).

2 Moffat, J. G., Vincent, F., Lee, J. A., Eder, J. & Prunotto, M. Opportunities and challenges in phenotypic drug discovery: an industry perspective. *Nature reviews Drug discovery* **16**, 531-543 (2017).

3 Tsai, J. M., Nowak, R. P., Ebert, B. L. & Fischer, E. S. Targeted protein degradation: from mechanisms to clinic. *Nature Reviews Molecular Cell Biology* **25**, 740-757 (2024).

4 Zwick, D., Vo, M. T., Shim, Y. J., Reijonen, H. & Do, J.-s. BACH2: the future of induced T-regulatory cell therapies. *Cells* **13**, 891 (2024).

5 May, E., Taylor, K., Gupta, L. & Miranda, W. Be Brave, Be Bold: Measuring the Return from Pharmaceutical Innovation. (Deloitte Centre for Health Solutions, 2025).

6 Vincent, F. *et al.* Phenotypic drug discovery: recent successes, lessons learned and new directions. *Nature Reviews Drug Discovery* **21**, 899-914 (2022).

7 Van Goor, F. *et al.* Rescue of CF airway epithelial cell function in vitro by a CFTR potentiator, VX-770. *Proceedings of the National Academy of Sciences* **106**, 18825-18830 (2009).

8 Naryshkin, N. A. *et al.* SMN2 splicing modifiers improve motor function and longevity in mice with spinal muscular atrophy. *science* **345**, 688-693 (2014).

9 Lemm, J. A. *et al.* Identification of hepatitis C virus NS5A inhibitors. *Journal of virology* **84**, 482-491 (2010).

10 Chung, C.-w. *et al.* Discovery and characterization of small molecule inhibitors of the BET family bromodomains. *Journal of medicinal chemistry* **54**, 3827-3838 (2011).

11 Liu, S. *et al.* Rational screening for cooperativity in small-molecule inducers of protein–protein associations. *Journal of the American Chemical Society* **145**, 23281-23291 (2023).

12 Scholes, N. S., Mayor-Ruiz, C. & Winter, G. E. Identification and selectivity profiling of small-molecule degraders via multi-omics approaches. *Cell Chemical Biology* **28**, 1048-1060 (2021).

13 Sun, J. *et al.* Recent advances in proteome-wide label-free target deconvolution for bioactive small molecules. *Medicinal Research Reviews* **41**, 2893-2926 (2021).

14 Jain, R., Subramanian, J. & Rathore, A. S. A review of therapeutic failures in late-stage clinical trials. *Expert Opinion on Pharmacotherapy* **24**, 389-399 (2023).

15 Geri, J. B. *et al.* Microenvironment mapping via Dexter energy transfer on immune cells. *Science* **367**, 1091-1097 (2020).

16 Oakley, J. V. *et al.* Radius measurement via super-resolution microscopy enables the development of a variable radii proximity labeling platform. *Proceedings of the National Academy of Sciences* **119**, e2203027119 (2022).

17 Knutson, S. D. *et al.* Micromapping (μMap) of HER2 Across Human Breast Cancers: Photocatalytic Proximity Labeling Identifies Primary Resistance Mechanisms and Functional Interactors. *bioRxiv*, 2025.2006. 2010.658685 (2025).

18 Huth, S. W., Geri, J. B., Oakley, J. V. & MacMillan, D. W. μMap-Interface: Temporal Photoproximity Labeling Identifies F11R as a Functional Member of the Transient Phagocytic Surfaceome. *Journal of the American Chemical Society* **146**, 32255-32262 (2024).

19 Suzuki, S. *et al.* Photochemical identification of auxiliary severe acute respiratory syndrome coronavirus 2 host entry factors using μMap. *Journal of the American Chemical Society* **144**, 16604-16611 (2022).

20 Seath, C. P. *et al.* Tracking chromatin state changes using nanoscale photo-proximity labelling. *Nature* **616**, 574-580 (2023).

21 Knutson, S. D. *et al.* Parallel Proteomic and Transcriptomic Microenvironment Mapping (μMap) of Nuclear Condensates in Living Cells. *Journal of the American Chemical Society* **147**, 488-497 (2024).

22 Pan, C., Knutson, S. D., Huth, S. W. & MacMillan, D. W. μMap proximity labeling in living cells reveals stress granule disassembly mechanisms. *Nature chemical biology* **21**, 490-500 (2025).
23 Trowbridge, A. D. *et al.* Small molecule photocatalysis enables drug target identification via energy transfer. *Proceedings of the National Academy of Sciences* **119**, e2208077119 (2022).
24 Huth, S. W. *et al.* μMap photoproximity labeling enables small molecule binding site mapping. *Journal of the American Chemical Society* **145**, 16289-16296 (2023).
25 Bissonnette, N. B. *et al.* μMap-FFPE: A High-Resolution Protein Proximity Labeling Platform for Formalin-Fixed Paraffin-Embedded Tissue Samples. *ChemRxiv* (2025).
26 Drewes, G. & Knapp, S. Chemoproteomics and chemical probes for target discovery. *Trends in biotechnology* **36**, 1275-1286 (2018).
27 Hill, J. R. & Robertson, A. A. Fishing for drug targets: a focus on diazirine photoaffinity probe synthesis. *Journal of medicinal chemistry* **61**, 6945-6963 (2018).
28 Homan, R. A. *et al.* Photoaffinity labelling with small molecules. *Nature Reviews Methods Primers* **4**, 30 (2024).
29 Yao, C. *et al.* BACH2 enforces the transcriptional and epigenetic programs of stem-like CD8+ T cells. *Nature immunology* **22**, 370-380 (2021).
30 Muto, A. *et al.* The transcriptional programme of antibody class switching involves the repressor Bach2. *Nature* **429**, 566-571 (2004).
31 Roychoudhuri, R. *et al.* The transcription factor BACH2 promotes tumor immunosuppression. *The Journal of clinical investigation* **126**, 599-604 (2016).
32 Dixon, A. S. *et al.* NanoLuc complementation reporter optimized for accurate measurement of protein interactions in cells. *ACS chemical biology* **11**, 400-408 (2016).
33 Buksh, B. F. *et al.* μMap-Red: proximity labeling by red light photocatalysis. *Journal of the American Chemical Society* **144**, 6154-6162 (2022).
34 Tomalka, J. A. *et al.* The transcription factor CREB1 is a mechanistic driver of immunogenicity and reduced HIV-1 acquisition following ALVAC vaccination. *Nature immunology* **22**, 1294-1305 (2021).
35 Song, Q., Mao, X., Jing, M., Fu, Y. & Yan, W. Pathophysiological role of BACH transcription factors in digestive system diseases. *Frontiers in Physiology* **14**, 1121353 (2023).
36 Schnoegl, D., Hiesinger, A., Huntington, N. D. & Gotthardt, D. AP-1 transcription factors in cytotoxic lymphocyte development and antitumor immunity. *Current Opinion in Immunology* **85**, 102397 (2023).
37 Thul, P. J. *et al.* A subcellular map of the human proteome. *Science* **356**, eaal3321 (2017).
38 MacDonald, B. T., Tamai, K. & He, X. Wnt/β-catenin signaling: components, mechanisms, and diseases. *Developmental cell* **17**, 9-26 (2009).
39 Wang, W. *et al.* FOXKs promote Wnt/β-catenin signaling by translocating DVL into the nucleus. *Developmental cell* **32**, 707-718 (2015).
40 Tang, Y. Y. *et al.* Effects of glycogen synthase kinase-3β inhibitor TWS119 on proliferation and cytokine production of TILs from human lung cancer. *Journal of Immunotherapy* **41**, 319-328 (2018).
41 Sivaprakasam, P. *et al.* Discovery of new acylaminopyridines as GSK-3 inhibitors by a structure guided in-depth exploration of chemical space around a pyrrolopyridinone core. *Bioorganic & medicinal chemistry letters* **25**, 1856-1863 (2015).
42 Söderberg, O. *et al.* Characterizing proteins and their interactions in cells and tissues using the in situ proximity ligation assay. *Methods* **45**, 227-232 (2008).
43 Maneix, L. *et al.* The mitochondrial protease LonP1 promotes proteasome inhibitor resistance in multiple myeloma. *Cancers* **13**, 843 (2021).
44 Gibellini, L. *et al.* Evidence for mitochondrial Lonp1 expression in the nucleus. *Scientific reports* **12**, 10877 (2022).

45 Gibellini, L. *et al.* Mitochondrial protease Lonp1 localizes to the nucleus in response to heat shock. (2021).
46 You, H. *et al.* Epstein-Barr virus–driven cardiolipin synthesis sustains metabolic remodeling during B cell transformation. *Science Advances* **11**, eadr8837 (2025).
47 Kingsley, L. J. *et al.* Structure-based design of selective LONP1 inhibitors for probing in vitro biology. *Journal of medicinal chemistry* **64**, 4857-4869 (2021).
48 Zanini, G. *et al.* Modulation of Lonp1 Activity by Small Compounds. *Biomolecules* **15**, 553 (2025).
49 San Chan, Y. *et al.* β-catenin functions as a molecular adapter for disordered cBAF interactions. *Molecular Cell* (2025).
50 Pollecker, K., Sylvester, M. & Voos, W. Proteomic analysis demonstrates the role of the quality control protease LONP1 in mitochondrial protein aggregation. *Journal of Biological Chemistry* **297** (2021).
51 Shin, C.-S. *et al.* LONP1 and mtHSP70 cooperate to promote mitochondrial protein folding. *Nature Communications* **12**, 265 (2021).
52 Li, J. *et al.* LONP1 regulation of mitochondrial protein folding provides insight into beta cell failure in type 2 diabetes. *Nature Metabolism*, 1-23 (2025).
53 Davis, M. I. *et al.* Comprehensive analysis of kinase inhibitor selectivity. *Nature biotechnology* **29**, 1046-1051 (2011).

## Methods

### Generation of C-terminal HiBiT HK-2 knock-in cell line

HK-2 cells were obtained from a colleague. CRISPR ribonucleoprotein (RNP) complexes were formed using 20pmol Cas9 protein (NEB) and 100 pmol sgRNA (Dharmacon) containing the target sgRNA sequence (5'AAAGAUUAUACCUAGUGACU3') and incubated 10 minutes at RT. $2x10^5$ cells in 20 µL Nucleofector solution SF with supplement added was then mixed with the RNPs, and then 200pmol ssODN HDR donor with end modifications (IDT) was added:

5'ACAGTGCCACAGGCTGACTGAAGAACGCCTGGATGGGAGAGGTGTGCGGACTGGGAGGCAGAGC
CGAGTCACTAGCTAATCTTCTTGAACAGCCGCCAGCCGCTCACGGTATAATCTTTCCTGGGCTGTTC
GTCAGTTGTACACTTATCAGTCATTTCCTGGCAGAAGTCCACGGTCACT3'

The entire mixture was electroporated in Nucleofector 16-well strips (LONZA) on the 4D Nucleofector system using pulse code CM-130. Cells were allowed to recover for several days then plated as single cells by limiting dilution. After expansion, clones were re-arrayed, replicated, and screened for luciferase signal using the NanoGlo HiBiT Lytic detection assay (Promega) and read on an Envision (Perkin-Elmer). Luciferase positive clones were expanded, genomic DNA isolated (Qiagen), and PCR was performed to amplify the C-terminus of BACH2 using primers (F: 5'- AACTGAAAGCATGCATGGGG-3' R: 5'- GTATTGCTGCTAAGACCGCTG-3'). PCR amplicons were purified using AMPureXP beads (Beckman-Coulter).

### Amplicon NGS:

Purified PCR amplicons were used as input for bead-linked transpososome tagmentation and normalization using the Illumina DNA Prep Kit according to the manufacturer's recommendations. Samples were uniquely indexed with up to 384 unique i5/i7 combinations using Illumina standard indexing kits and amplification was carried out with an initial 98 °C 3 min step, then 6 cycles of 98 °C 45 s, 62 °C 30 s, 68 °C 2 min, followed by a 2 min final extension at 68 °C and cooled to 10°C. Samples were next pooled, then double-sided size selected using Illumina purification beads first with 0.6 v/v ratio beads to bind and remove larger fragments, then with 0.11 v/v ratio beads to wash out smaller fragments, and finally eluted with resuspension buffer. The eluted library was quantitated using the Qubit 1X dsDNA HS assay (ThermoFisher), run on a Tapestation HSD1000 (Agilent), diluted to 4 nM, denatured, and diluted to 8 pM following Illumina's standard protocol with 1% v/v PhiX as a spiked in control. MiSeq run parameters were set at 150bp paired-end, dual indexed using a 300v2 micro reagent kit (Illumina).

Samples were demultiplexed using bcl2fastq v2.2.0 and ran though the CRISPR-DAV analysis pipeline as previously described (1):

(1): Wang X, Tilford C, Neuhaus I, Mintier G, Guo Q, Feder JN, et al. CRISPR-DAV: CRISPR NGS data analysis and visualization pipeline. Bioinformatics. 2017;33:3811–3812. doi: 10.1093/bioinformatics/btx518.

Amplicon NGS analysis showed selected clones to be homozygous for the HiBiT KI. NanoGlo HiBiT Luciferase assay was repeated on this clone and showed 2,887 RLU / 50k cells compared to 309 RLU for HK-2 parental (9-fold signal window).

**HiBiT and cytotoxicity assays**

Cell cultures were grown in tissue-culture treated polystyrene 175 $cm^2$ flasks containing Dulbecco's Modified Eagle Medium (DMEM) supplemented with 10% heat-inactivated fetal bovine serum, and 1X Antibiotic-Antimycotic. Cultures were maintained in growth-phase with twice-weekly passaging to prevent confluency. Passaging of cells was performed by washing monolayers twice with Dulbecco's phosphate-buffered saline without divalent cations then treating with 0.05 Trypsin-EDTA solution for 2-3 minutes. Trypsin-EDTA was neutralized with the addition of growth media containing 10% FBS. All cell culture reagents were obtained from Gibco (Pittsburgh, PA). Compounds were dissolved and serially diluted in 100% DMSO (Sigma Aldrich, St Louis, MO) before being transferred to 1536-well assay plates using an Echo acoustical liquid handler (LABCYTE, San Jose, CA). Cells were harvested from T-175 flasks as described above and counted using Moxi Cyte Single Color Viability Reagent (Orflo, El Cajon, CA). Cells were centrifuged at 300 x *g* for 10 minutes and resuspended in DMEM without phenol red media supplemented with 5% heat-inactivated fetal bovine serum, 1X Antibiotic-Antimycotic, and 25 mM HEPES. Cells were dispensed into white 1536-well, tissue cultured treated plates containing serial diluted compounds before being incubated at 37 °C, 5% $CO_2$, 95% relative humidity for 24 hours. The next day, plates were removed from the incubator and equilibrated to room temperature for 10 minutes before adding NanoGlo HiBiT Lytic reagent according to the manufacturer's protocol (Promega, Madison, WI). For compound cytotoxicity assessment, duplicate assay plates prepared in parallel were removed from the incubator and treated with CellTiter Glo reagent according to manufacturer's recommended protocol (Promega, Madison, WI). To assess proteasome dependence, cells were treated with 2.5–5 µM MG-132 (Selleckchem, Houston, TX) before being added to assay plates containing compounds and incubated for 24 hours. Luminescence from assays described above was measured using an Envision plate reader (Perkin-Elmer, Shelton, CT). The percent inhibition was calculated relative to DMSO controls, and the half-maximal inhibitory concentration ($IC_{50}$) was calculated using a 4-parameter logistic equation.

**BACH2 degradation in Jurkats**

Jurkat cells were obtained from ATCC and maintained in RPMI-1640 medium (Gibco) supplemented with 10% FBS, 1% Penicillin-Streptomycin, and 1 mM Sodium Pyruvate in a humidified incubator at 37 °C with 5% $CO_2$. $1x10^7$ cells were dispensed into 6-well, tissue culture treated plates containing serial diluted compounds before being incubated at 37 °C, 5% $CO_2$, for 16-18 hours. Cells were collected from each well and whole cell lysate was prepared using 1X RIPA (Sigma). Quantification of lysate was determined via BCA method (Thermo Fisher). For pre-treatment with LONP1-IN-2 (MedChem Express), $1x10^6$ cells were dispensed into 6-well, tissue culture treated plates containing vehicle or 1 µM inhibitor before being incubated at 37 °C, 5% $CO_2$. After 24 hours, wells were directly spiked with a final concentration of 20 µM of each BACH2 degrader compound and incubated at 37 °C, 5% $CO_2$, for 16-18 hours and collected as described earlier.

**Western blotting**

Electrophoresis was performed using Novex™ WedgeWell™ 4 to 20%, Tris-Glycine precast gels and a XCell SureLock Mini-Cell Electrophoresis System (Thermo Fisher). After electrophoresis, gels were transferred to nitrocellulose membranes using an iBlot 2 Gel Transfer Device (Invitrogen) at 25V for 10 minutes. The membranes were then blocked in 5% bovine serum album (BSA) in Tris-buffered saline + 0.05% Tween20 (TBST) and incubated for 1 hour at room temperature with agitation. The blocking solution was then decanted and replaced with a primary antibody solution in blocking buffer and incubated overnight at 4 ºC with gentle rocking. Membranes were then washed with 1X TBST (3 x 5 min) before incubation with a secondary antibody solution followed by imaging via Licor Odyssey CLx scanner. For BACH2 degradation assays, 30 µg treated Jurkat whole cell lysate was used per lane, and BACH2 detected with mouse primary antibody at 1:100 overnight (BioLegend, 16B10B53) and anti-tubulin (CST 2418, 1:1000). Other primary antibodies used for western blot analyses: anti-HECTD3

(ProteinTech 11487-1-AP, 1:1000), anti-β-catenin (CST 8480,1:1000), anti-active β-catenin (CST D13A1, 1:1000), anti-GSK3β (CST 9315S, 1:1000), anti-Actin (Thermo Fisher MA1-744, 1:10,000). Secondary antibodies from Licor were used for all blot analyses (Goat anti-Rabbit IRDye800 Licor 926-32211 and Goat anti-Mouse IRDye680 Licor 926-68070).

**Preparation of catalyst-antibody conjugates**

Antibody conjugates were prepared as described previously.[25,33] 500 µg of Goat anti-Rabbit IgG (Thermo Fisher 31210) was first buffer exchanged using Amicon Ultra-Centrifugal Filters (Millipore, UFC501096) into 0.1 M Carbonate/BiCarbonate buffer, pH 9.2. Separately, a 5 mM solution of Sn Chlorin DBCO was prepared in DMSO. 20 µL of this solution was then reacted with 10 µL of a 10 mM solution of azido-$PEG_{12}$-NHS ester (BroadPharm, BP-21607) in DMSO. After incubating in the dark for 1 hour, 15 µL of this mixture was then reacted with 500 µg of buffer-exchanged antibody in a total volume of 250 µL and allowed to incubate with end-over-end rotation for 1 hour protected from light. Crude conjugation reactions were then purified using 2 mL Zeba™ Spin Desalting Columns, 40K MWCO (Thermo Fisher, 87768) after equilibrating in 1X DPBS. Purified conjugated antibodies were first characterized by Pierce™ 660nm Protein Assay Reagent (Thermo Fisher 22660) versus a bovine serum albumin standard curve. Catalyst loading was determined by comparing the absorbance of conjugates at 410 nm (vs a Sn chlorin DBCO standard curve in PBS). Conjugation reactions typically yielded catalyst loading rates of ~1-3 catalysts per antibody.

**BACH2 µMapX**

Jurkat cells were harvested and $1x10^7$ cells were dispensed into 6-well, tissue culture treated plates containing 10-20 µM compounds or 0.01% DMSO before being incubated at 37 °C, 5% $CO_2$, for 16-18 hours. A 50 mg/mL solution of 3,3′-Dithiodipropionic acid di(N-hydroxysuccinimide ester) (DSP) crosslinker (Sigma D3669) was prepared in 100% anhydrous DMSO and then diluted to a working concentration of 0.5 mg/mL in 1X DPBS. Jurkat cells were pelleted at 300 x *g* for 5 minutes and resuspended in ~1.5 mL DSP working solution in 2 mL Lo-bind tubes (Eppendorf) and incubated at room temperature with rotation for 20 min. Crosslinking was quenched by spiking in 100 µL of 2.5M glycine and incubating for 5 minutes with gentle rotation. Cells were then permeabilized by addition of 20 µL 10% Triton X-100 (0.1% final) and incubated at room temperature for 15 minutes with rotation. 200 µL 10% BSA was then added to each tube (1% final) and cells were pelleted at 800 x *g* for 10 minutes. Pellets were resuspended in 1.5 mL of 3% BSA, 0.05% Tw20 in DPBS and incubated with gentle rotation at room temperature for 45 minutes. 10 µL BACH2 primary antibody (CST, D3T3G, Rabbit) or rabbit isotype control ( initial validation, Thermo Fisher 02-6102) was then added to each tube with gentle rotation for another hour. Cells were pelleted at 800 x *g* for 10 minutes and washed twice with 2 mL 0.05% Tw20, 1% BSA in DPBS with end-over-end rotation for 5 minutes each wash. Cells were then resuspended in 1.5 mL of a secondary antibody solution (Goat anti-rabbit Sn chlorin 1 µg/mL) in 0.05% Tw20, 3% BSA in DPBS. Samples were incubated at room temperature protected from light for at least an hour. Cells were pelleted at 800 x *g* for 10 minutes and washed twice with 2 mL 0.05% Tw20, 1% BSA in DPBS with end-over-end rotation for 5 minutes each wash. Cells were then resuspended in 1.8 mL of a 1 mM solution of biotin-aniline solution in DPBS + 0.05% Tw20 and incubated at room temperature protected from light for ~ 10 minutes. Tubes were placed in a reflector cone placed above a custom assembled Chanzon 1DGL-JC-100W-660 100 W LED (650-660 nm)[33] and irradiated for 20 minutes in a cold room. Every 10 minutes, tubes were inverted several times to resuspend any settled cells. 200 µL 10% BSA was then added to each tube (1% final) and cells were pelleted at 800 x *g* for 10 minutes and washed twice with 2 mL 0.05% Tw20, 1% BSA in DPBS with end-over-end rotation for 5 minutes each wash. Cells were pelleted once more and resuspended in 1 mL lysis buffer (1X RIPA + 0.5% SDS, 10 mM sodium ascorbate, and 50 mM DTT). Samples were incubated for 5 minutes and then sonicated using a Branson tip sonicator for 15s at 35% intensity. Tubes were then incubated at 37 ºC for at least 1 hour with rotation. The samples were centrifuged at 16,000 x *g* for 15 min at 4 °C. The lysates were then centrifuged at 16,000 x *g* to pellet any insoluble material, and the supernatants transferred to a new tube. For streptavidin bead enrichment, lysate was added to a 15 mL conical tube containing 4 mL 1X RIPA and 100 µL of Pierce streptavidin magnetic beads that were pre-washed twice with 1 mL RIPA buffer. The samples were incubated overnight on a rotisserie at 4 ºC, and the beads were pelleted on a magnetic rack and condensed into a single 1.7 mL Axygen tube for each replicate. The supernatant was removed, and the beads were washed 3x with 1 mL 1% SDS in DPBS, 3x with 1 mL 1M NaCl in DPBS, 3x with 1 mL 10% EtOH in DPBS, and 3x with 1 mL 100 mM $NH_4HCO_3$. The beads were then resuspended in 500 µL 6 M urea in DPBS and 25 µL of 200 mM DTT in 25 mM $NH_4HCO_3$ was added. The beads were then incubated at 55 ºC for 30 minutes on a rotator. Subsequently, 30 µL 500 mM iodoacetamide (IAA) in 25 mM $NH_4HCO_3$ was added and

incubated for 30 min on a rotator at room temperature in the dark. The supernatant was removed, and the beads were washed 3x with 0.5 mL DPBS followed by 3x with 50 mM $NH_4HCO_3$. Beads were then resuspended in 40 µL 50 mM Ammonium Bicarbonate buffer containing 1 µg MS-grade trypsin per sample and digested at 37 ºC overnight with rotation. Trypsin was then quenched with 1 µL Optima LC/MS Formic Acid and supernatants were passed through a 0.22-micron spin filter column (CoStar, 98231-UT-1) before being transferred to an LC/MS vial for proteomics analysis.

**BACH2 µMap TargetID**

Jurkat cells ($1x10^7$ cells) were dispensed into 1.7 mL low-bind tubes (Axygen) in a total volume of 1 mL RPMI-1640 media + 10% FBS without phenol red. In triplicate tubes, either Ir-$PEG_3$-NHBoc, BMS906941-Ir or 5-Ir conjugate was added from a 2 mM (1000X) stock in DMSO to a final concentration of 2 µM. Tubes were then incubated with rotation at 37 ºC, protected from light, for 30 minutes. Cells were then pelleted at 500 x g for 5 minutes and resuspended in 250 µM biotin-$PEG_3$-diazirine solution in complete RPMI-1640 media without phenol red. Tubes were then incubated with rotation at 37 ºC, protected from light, for 30 minutes. Tubes were then placed above a Penn PhD Photoreactor M2 integrated photoreactor and irradiated for 3 minutes at 100% intensity. After irradiation, cells were pelleted and washed twice with 1 mL DPBS and pelleted once more. This was then resuspended in 1 mL of 1X RIPA and sonicated at 35% power for 10 seconds. Samples were then centrifuged at 17,000 × *g* for 10 minutes at 4 ºC to pellet cell debris. The supernatant was transferred to a new tube. For streptavidin bead enrichment, clarified cell lysate was added to a 1.7 mL Axygen tube containing 100 µL of Pierce streptavidin magnetic beads that were pre-washed twice with 1 mL RIPA buffer. The samples were incubated overnight on a rotisserie at 4 ºC, and the beads were pelleted on a magnetic rack. The supernatant was removed, and the beads were washed 3x with 1 mL 1% SDS in DPBS, 3x with 1 mL 1M NaCl in DPBS, 3x with 1 mL 10% EtOH in DPBS, and 3x with 1 mL 100 mM $NH_4HCO_3$. The beads were then resuspended in 500 µL 6 M urea in DPBS and 25 µL of 200 mM DTT in 25 mM $NH_4HCO_3$ was added. The beads were then incubated at 55 ºC for 30 minutes on a rotator. Subsequently, 30 µL 500 mM iodoacetamide (IAA) in 25 mM $NH_4HCO_3$ was added and incubated for 30 minutes on a rotator at room temperature in the dark. The supernatant was removed, and the beads were washed 3x with 0.5 mL DPBS followed by 3x with 50 mM $NH_4HCO_3$. Beads were then resuspended in 40 µL 50 mM Ammonium Bicarbonate buffer containing 1 µg MS-grade trypsin per sample and digested at 37 ºC overnight with rotation. Trypsin was then quenched with 1 µL Optima LC/MS Formic Acid and supernatants were passed through a 0.22-micron spin filter column (CoStar, 98231-UT-1) before being transferred to an LC/MS vial for proteomics analysis.

**Quantitative mass spectrometry proteomics and data analysis**

Label-free, data-independent acquisition (DIA) proteomics was performed on a Bruker TimsTOF Pro 2 connected to a nanoElute LC. For each sample, ~100 ng of protein was injected onto a trap column (C18 Pepmap, 5 µM particle size, 5 mm length, 300 µM internal diameter), followed by separation via an analytical column (C18 ReproSil AQ, 1.9 µM particle size, 100 mm length, 75 µM internal diameter). Peptides were eluted via an acetonitrile/water gradient at a column temperature of 40 °C (buffer A = 0.1% formic acid/water, buffer B = 0.1% formic acid/acetonitrile; flow rate 0.5 µL/min; gradient: start at 2% B, then increase to 35% B over 20 min, increase to 95% B over 0.5 min, hold at 95% for 2.25 min). Scans were performed in positive ion, dia-PASEF mode over a m/z range of 100-1700 with a ramp time of 100 ms, Accu. time of 100 ms, and a duty cycle of 100%, ramp rate of 9.43 Hz, MS averaging set to 1. Absolute thresholds were set to 5000 for mobility peaks and 10 for MS peaks. Data were collected with Bruker Compass HyStar v6.2. Raw data (.d files) were then processed via DIA-NN 1.8.1 via the following parameters: trypsin/P digestion, 3 missed cleavages, 3 max. variable modifications, N-term M excision, Ox(M), Ac(N-term) and C-carbamidomethylation, peptide length range of 7-30, precursor charge range 1-4, m/z range 300-1800, fragment ion range 200-1800, Mass accuracy and MS accuracy both set to 10, precursor FDR set to 1%. Within the DIA-NN algorithm, the following settings are applied: “Use isotopologues”, “MBR” (match between runs), “No shared spectra”, “Heuristic protein inference”. A spectral library was utilized which was generated in DIA-NN from all known human proteins (In-Silico spectral library – generated in DIA-NN via FASTA of Uniprot human proteome UP000005640 – options selected were “FASTA digest for library-free search/library generation” and “Deep learning-based spectra, RTs and IMs prediction”, other parameters same as described above). After processing, the resulting matrix.pg files were analyzed in Perseus (v 2.0.7.0)[71], where intensities are inputted as “main” while the other descriptors are listed as “categorical”. Intensities were transformed by log base 2, and data was annotated to group by the appropriate condition. Missing values were then replaced from a normal distribution (width = 0.3, downshift = 1.8, separately for each column). Normalization was

performed via median subtraction, and a volcano plot was generated utilizing a t-test for statistical significance. Resulting volcano plots were plotted in GraphPad Prism 10 for final figures. Gene ontology analysis was performed on Metascape v3.5.

**Generation of Jurkat knockout cell lines**

Jurkat Clone E6-1 cells were obtained from ATCC. CRISPR ribonucleoproteins (RNPs) were formed using 20pmol Cas9 protein (IDT Alt-R™ S.p. HiFi Cas9 Nuclease V3) and 100 pmol sgRNA (IDT) containing the target sequences listed in the supplementary tables where appropriate and incubated for 10 minutes at room temperature. $2x10^5$ cells were pelleted and re-suspended in 20 µL Nucleofector solution SE with supplement added (Lonza) for each transfection, mixed with the ribonucleoprotein complexes, electroporated in 16-well cuvettes using pulse code CL-120, then transferred to 12-well plates. Cells were allowed to recover and expanded for approximately 1 week. Pools were next evaluated for NHEJ InDels by amplicon sequencing as described earlier and then seeded for single cell by limiting dilution method. Following expansion, clones were re-arrayed, replicated, and screened for frame-shifting NHEJ InDels by sequencing. Briefly, clones were replicated, pelleted, and lysed with 20 µL QuickExtract buffer (LGC) by heating at 65 ºC for 6 minutes then 98 ºC for 2 minutes. 2 µL lysate was used for PCR in 50 µL reactions using Kapa HiFi HotStart ReadyMix (Roche) and locus specific primers (supplemental tables) and subjected to 32-cycles of PCR. PCR amplicons were purified using 90 µl AMPureXP beads (Beckman Coulter), washed twice with 70% ethanol, eluted with 15 µl TE buffer, and checked on a Fragment Analyzer (Agilent). Amplicon NGS was then performed as described earlier.

**qPCR**

Jurkat cells were harvested and $1x10^7$ cells were dispensed into 6-well, tissue culture treated plates containing 10-20 µM compounds or 0.01% DMSO before being incubated at 37 °C, 5% $CO_2$, for 16-18 hours. Cells were collected from each well and pelleted at 300 x *g* for 5 minutes. Cells were washed gently in 1 mL DPBS and pelleted once more. Total RNA was then isolated using the Monarch Total RNA Miniprep Kit (New England Biolabs). RNA was eluated in a total volume of 100 µL nuclease-free water and quantified via Nanodrop. 1 µg total RNA was then mixed with 20 pmol reverse primer in a total volume of 8 µL nuclease-free water and heated to 70 ºC for 10 minutes. 10 µL ProtoScript II Reaction Mix (New England Biolabs) and 2 µL ProtoScript II Enzyme Mix was added and incubated at 42°C for one hour. Reactions were then inactivated at 80 ºC for 5 minutes. qPCR reaction mixes as were prepared in duplicate (10 µL each) for each RT reaction by combining with 10 µL iTaq Green Supermix (2X) with 10 pmol each of forward and reverse primers in a total volume of 20 µL nuclease-free water. Reactions were monitored using a Roche Lightcycler 96 instrument with the following thermocycler conditions: initial denaturation at 94 °C for 3 minutes, followed by 45 cycles of 15 second denaturation at 94 ºC, annealing at 60 ºC for 30 seconds, and extension at 68 ºC for 30 seconds, followed by a 5 minute final extension at 68 ºC. The relative quantification of transcript levels was determined using the comparative Ct (ΔΔCt) method. The cycle threshold (Ct) value for BACH2 in each sample was normalized to the Ct value of the endogenous control, GAPDH, to obtain the ΔCt value. The ΔCt value for each experimental sample (e.g., compound-treated) was then normalized to the average ΔCt of the control samples (DMSO) to calculate the ΔΔCt value. The fold change in *BACH2* mRNA expression relative to the control was calculated using the formula $2^{-\Delta\Delta Ct}$.

**Immunofluorescence Microscopy**

Jurkat cells ($1x10^7$) were dispensed into 6-well, tissue culture treated plates containing 20 µM compounds or 0.01% DMSO before being incubated at 37 °C, 5% $CO_2$, for 16-18 hours. 50,000 cells were then dispensed into replicate wells of glass-bottom 24-well plates pre-coated with 0.01% poly-L-lysine and centrifuged at 400 x g for 10 minutes in a swinging bucket rotor. Media from each well was carefully aspirated and cells were then fixed with 4% paraformaldehyde in DPBS for 15 minutes at room temperature, washed once with DPBS, and then permeabilized with 0.1% Triton X-100 in DPBS for 10 minutes. Samples were then incubated at room temperature for 1 hour in blocking buffer (3% BSA, 0.05% Tween20 in DPBS). A primary antibody solution (BACH2 rabbit antibody CST D3T3G, 1:200; β-catenin mouse antibody, Thermo Fisher, 13-8400 1:500; LONP1 rabbit antibody, ProteinTech, 15440-1-AP, 1:1000 ; COXIV mouse antibody, Thermo Fisher, MA5-15686, 1:1000) was then prepared in blocking buffer and applied for at least 1 hour at room temperature. Samples were then washed 3X with 0.05% Tw20 in DPBS and stained with a secondary antibody solution in Blocking buffer for 1 hour at room temperature. DAPI (1:10000) was used for nuclear staining, goat anti-rabbit Alexa Fluor 488 (1:1000) and goat anti-mouse Alexa Fluor 555 (1:1000) were used to target specific primary antibodies. Finally, samples were washed 3X with 0.05% Tw20 in DPBS and stored in DPBS before imaging. Samples were imaged using NIS Elements AR v4.60.00 software on

a Nikon A1R-Si HD Confocal Microscope. Image processing was performed with ImageJ2/FIJI Mac OS X software.

**Proximity ligation assay**

Jurkat cells ($1x10^7$) were dispensed into 6-well, tissue culture treated plates containing 20 μM compounds or 0.01% DMSO before being incubated at 37 °C, 5% $CO_2$, for 16-18 hours. 10,000 cells were then dispensed into replicate wells of glass-bottom 96-well plates pre-coated with 0.01% poly-L-lysine and centrifuged at 400 x g for 10 minutes in a swinging bucket rotor. Media from each well was carefully aspirated and cells were then fixed with 4% paraformaldehyde in DPBS for 15 minutes at room temperature, washed once with DPBS, and then permeabilized with 0.1% Triton X-100 in DPBS for 10 minutes. Samples were then incubated at room temperature for 1 hour in blocking buffer (3% BSA, 0.05% Tween20 in DPBS). A primary antibody solution (BACH2 rabbit antibody CST D3T3G, 1:200; β-catenin mouse antibody, Thermo Fisher, 13-8400) was then prepared and added to each well. Plates were incubated for at least 1 hour at room temperature. Each well was then washed 3x with DPBS and then incubated with an appropriate PLA probe solution (Goat anti-Mouse PLUS or Goat anti-Rabbit MINUS) that was diluted 1:5 in 3% BSA in DPBS. Plates were incubated at 37 ºC for at least an hour, followed by a 5 minute incubation with 1X Wash Buffer A. Wells were then treated with ligase (1:40 in 1X ligation buffer) and incubated at 37 ºC for 30 minutes. After 2x5 minute washes with 1X Wash Buffer A, wells were incubated with polymerase (1:80 in 1X amplification buffer) at 37 ºC for 100 minutes. Wells were washed twice with 1X Wash Buffer B for 10 minutes followed by one wash with 0.01X Wash Buffer B. After airdrying wells for 5 minutes, they were then covered with a minimal amount of Duolink In Situ Mounting Medium. Samples were imaged using NIS Elements AR v4.60.00 software on a Nikon A1R-Si HD Confocal Microscope. Image processing was performed with ImageJ2/FIJI Mac OS X software.